IEEE Access
Multidisciplinary | Rapid Review | Open Access Journal

Received 16 November 2023, accepted 30 November 2023, date of publication 1 December 2023,
date of current version 29 December 2023.

Digital Object Identifier 10.1109/ACCESS.2023.3338746

RESEARCH ARTICLE

Prostate Segmentation on Magnetic Resonance Imaging

CHENGJUAN REN[1] AND HUIPENG REN[2]
[1]College of Language Intelligence, Sichuan International Studies University, Chongqing 400031, China
[2]Department of Medical Imaging, Baoji Central Hospital, Baoji 721099, China

Corresponding author: Chengjuan Ren (enchengjuan163@163.com)

This work was supported in part by the Science and Technology Research Project of the Chongqing Education Commission under Grant KJQN202300901, and in part by the Sichuan International Studies University 2023 Planning Project under Grant sisu202306.

ABSTRACT Automatic and precise segmentation of the prostate is beneficial to various diagnostic and therapeutic procedures on magnetic resonance imaging. However, the work is very challenging because of the heterogeneity of prostate tissue, the lack of clearly defined boundaries, and the wide variation in prostate shape between individuals. Based on the segmentation scheme for the prostate and its lesion regions, a new deep convolution neural network is proposed in this research. To acquire excellent segmentation performance with consistency in both appearance and space, CRF-RNN is added on top of the network. By introducing an attention mechanism, the network is made to focus more feature on the prostate zones in both channel and spatial dimensions. In addition, a new dense block is created to stabilize parameter updates and prevent gradients from disappearing as the network deepens. Finally, the model was trained and validated using the real prostate dataset of 180 patients with four cross-validations. The proposed model achieves 95% HD, 86.82%, 93.90%, 94.11%, 93.8%, 7.84% for prostate, 79.2%, 89.51%, 88.43%, 89.31%, 8.39% for lesion area in segmentation in terms of IOU, Dice score, accuracy, and sensitivity. Compared to the state-of-the-art models FCN, U-Net, U-Net++ and ResU-Net, the segmentation model shows more promising results. With an outstanding achievement in automated segmentation of prostate and lesion regions, the presented model highlights the ability of the novel deep convolutional neural network to facilitate clinical disease intervention and management.

INDEX TERMS Dense block, magnetic resonance imaging, convolution neural network, attention mechanism, CRF-RNN.

I. INTRODUCTION

Prostate cancer (PCa) is a very frequent disease in most men, accounting for about one in two cases and is the fifth most common cause of death worldwide. [1]. It is a very late age of incidence until 55 years and gradually increases with a peak age of 70 to 80 years. The time of onset is slightly earlier in patients with familial hereditary prostate cancer, with 43% of patients aged less than 55 years [2]. For the diagnosis, treatment and follow-up of prostate cancer, transrectal ultrasound (TRUS), magnetic resonance imaging (MRI) and computed tomography (CT) are the main imaging modalities available.

The associate editor coordinating the review of this manuscript and approving it for publication was Santosh Kumar.

Conventional segmentation efforts for prostate or lesion areas have involved outline and appearance, geographic, and some mixed methodologies. Prostate margins or borders are enforced on prostate segmentation. For example, by fully exploiting the additional knowledge encoded in the different layers of a convolutional neural network (CNN) to improve prostate segmentation in the TRUS. Wang et al. [3] built a deep neural network fitted with a depth attention function module. Brosch et al. [4] reformulated boundary recognition as a regression problem, in which we can set a convolution neural network to estimate distribution of distances between surface meshes and their associated boundary points.

For accurate segmentation of the prostate and its lesion regions, manual segmentation continues to be the most

widely used method. This is an extremely time-consuming task, which varies from company to company. This may result in poor repeatability and increased observer variability. Reliable automated segmentation of the prostate and its lesion regions is therefore urgently needed in daily clinical practice.

Today, CNN is gaining ground in medical imaging, having achieved results in many image classification and segmentation works [5], [6], [7]. One of the distinguished flagship works, Ranneberger et al. [8], suggested the U-Net and fully exploited the scarce and precious feature to improve the estimation performance. Instead of a simple binary classification, the U-shaped structure enables precise detection of medical images. The entire U-Net process consists of encryption and decryption, only a convolution layer without a full connection layer. U-Net is probably the hottest segmented network. Isensee et al. [9] argued that a common U-Net can meet the needs of all segmentation problems and only one image pre-processing and post-processing for all segmentation problems are needed. As a result, nnUNet was proposed to develop detailed guidelines for the entire segmentation process of image pre-processing, network training and image post-processing. Rajchl et al. [10] proposed interactions based on enclosing boxes or underlining, but they treated the results of these interactions as weak annotations for segmentation rather than being used to guide segmentation. Top et al. [11] then further combined active learning and interactive approaches to allow physicians to correct for areas of uncertainty and help mold better feature selection. Wang et al. [12] improved segmentation performance by treating user interaction information as a new channel of the image and feeding it directly into the new model. Geng et al. [13] showed the multiple-channel feature pyramid structure to handle multiple-scale feature mapping, where each layer controls the scale of the channels through the SE module to enhance the edge features of the prostate. The feature map output from the MFPN was fed into the region proposal network to get the final results.

For the prostate and its diseased regions, it is very demanding to obtain a high-performance automatic segmentation model. The blurring of tissue boundaries within the image renders it impossible to discriminate them from the surrounding dissimilar prostate tissue, further leading to under or over-segmentation [14]. Finally, the fact that diverse individuals typically come in various sizes and shapes of prostate gland poses a problem for modeling universal learning. The above-mentioned factors contribute to the difficulty of resecting regions of prostate cancer. A new network is suggested in this work for the efficient segmentation of the prostate and prostate cancer region. The stem of the network is informed by the U-Net. We increase a straightforward but powerful attention module that can be applied extensively to improve the representational power of CNNs. The attention network is responsible for concentrating attention on some important features of the image, thus improving the quality of the segmentation. To mitigate the disappearance of gradients and to increase the prevalence of characteristics in the model, a new dense block is also used. The dense block allows the network to be characterized by the more abstract features that are of interest to us. Data augmentation is used to address overfitting of the model due to a lack of data during the data preparation phase. The principal components of this work are as follows:

1) To achieve pixel-wise detection, a new CNN model is presented in the work. The network utilizes lengthy and skips connections between the opposing stages.
2) To raise the semantic level of segmentation, a mean-field approximation as a recurrent neural network is embedded into our model.
3) To maintain more efficient prostate features by stabilizing parameter updates, a new dense block is added, using short-hop connections between different convolution layers.
4) CBAM allows for a better model focus on prostate and lesional characteristics, both spatial and canalicular. By learning which information to emphasise and which to suppress, the model supports the flow of information within the network.
5) The final step is the evaluation of the validity of the proposed model on a real-world dataset. For several evaluation metrics, the performance of the model is superior to the advanced segmentation model.

II. MATERIALS AND METHODS

A. DATASETS

Data was centrally collected between January 2018 and May 2021. A total of 180 patients (122 healthy and 58 prostate cancer patients) were scanned on the GE 3.0T 750 MR. All patients gave informed consent for data collection. The DWI format was used as input in our model. To ensure the accuracy of the annotated data, we invited six experienced urologists to participate in data collation and annotation before and after. The specific division of labor was that three clinicians with 5 years of experience spent 3 months annotating the segmented region. The other three specialists examined and corrected the annotated regions.

B. DATA PRE-PROCESSING

Due to the small amount of data, data enhancement was used during the experiment. Data enhancement was performed by rotating an image to 4 angles (0,30,60, 90); randomly merging the central regions of 3 images into one image; and zooming in or out. The data preprocessing stage also contains a normalization operation of the data to converge the data to a point as soon as possible. Linear scaling, also known as minimum-maximum scaling, is a linear variation of the original data, scaling the data between [0,1].

$$X' = \frac{x - \min(x)}{\max(x) - \min(x)} \tag{1}$$

This preserves the relationships present in the original data and is the easiest method for eliminating magnitude and scatter effects.

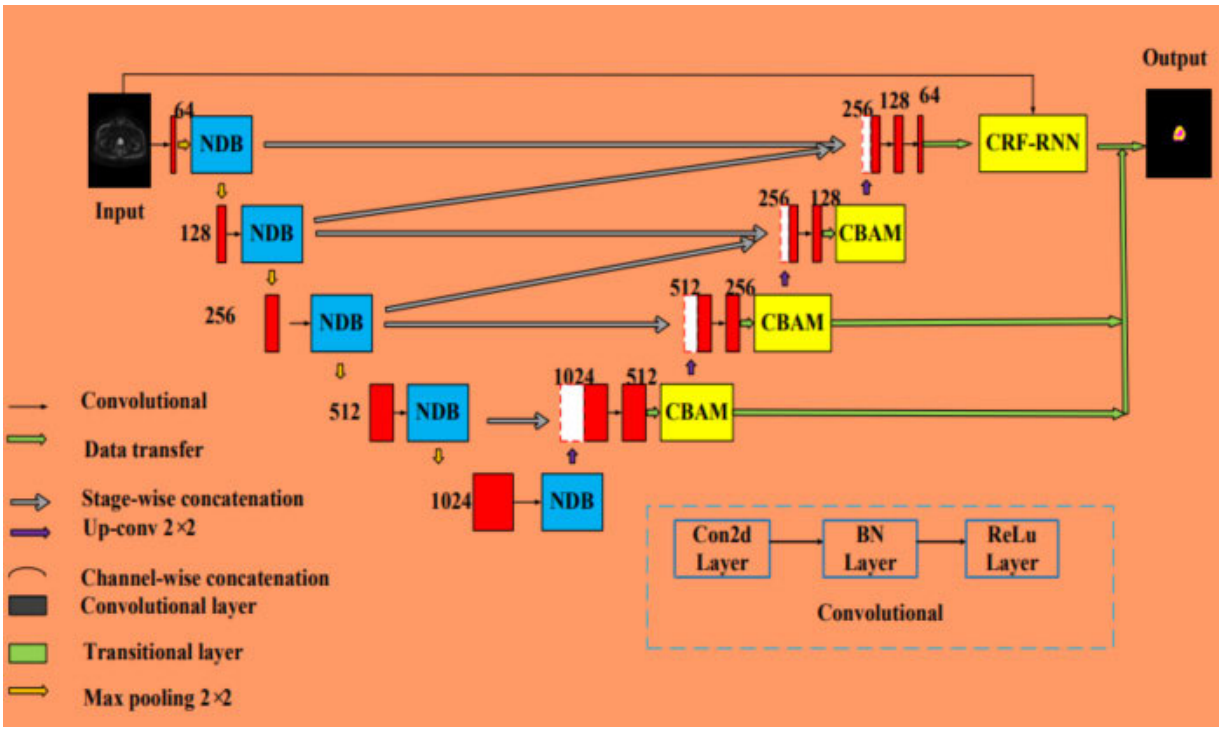

FIGURE 1. Structure of the proposed (our) method. The model is coloured yellow for the CBAM module, dark blue for the new dense block (NDB), with CRF-RNN at the end of the model.

III. THE PROPOSED MODEL

Our model is supported by the classic U-Net framework [8], [15] and is known as encoder-decoder concept. Some modules are introduced in the model, including a new dense block (NDB), convolution block attention module (CBAM), and conditional random fields as recurrent neural networks (CRF-RNN) [16] to capture more feature representation in segmentation. Characteristics from the shrinkage path have been combined into the expansion path at the symmetry and asymmetry levels to exploit the flat information. Figure 1 shows the detailed design of the proposed scheme. Input of the model is a DWI image of the prostate. Convolving operations within the model are all performed using the 3×3 shown in red. The model comprises a contractile (left) and expansive (right) path. The contractile pathway produces contextual information, and the expansive pathway provides precise positioning. The entire architecture supports continuous parameter tuning with short jump links between the various convolution layers in every step. Long and short skip connections are combined to increase overall network efficiency [17]. The contraction path, which is the stage where the downsampling takes place, raises the total to 1024 channels, up from 64. Convolution, ReLU, dense block and 2×2 max-pooling are used in each step of the contraction path. By upsampling and reducing the number of channels from 1024 to 64, the expansion path gradually regains its original size. Each increment in the growth path consists of an up-convolution of the featured prostate map, then a 2×2 convolution that halves the number of feature points, a linking with the tailored prostate feature from the same level's contraction path, and two 3×3 convolutions, each positing a ReLU, a CBAM. To obtain the number of classes, three convolutions and a spatial pyramid pooling at different rates (6, 12, 18) are performed in the latter layer. Since border pixels are dropped in each convolution. The NDB [18], which comprises batch normalization, the ReLU layer, and the convolution layer, is a dense concatenation of numerous composite functions. It is designed to mitigate gradient disappearance and improve the spreading of the prostate and its lesion features for recycling in the following network layer.

A. THE NEW DENSE BLOCK

The suggested dense block is built on the concept of dense, residual and transition blocks. The skip connection is called a new dense block. (NDB), Figure.2. Thus, these combined nonlinearities in the two subsequent blocks undergo transformations, which are walked around by a skipped connection [19]. b_i is the input of the network, then the output is defined as:

$$x_0 = A(b_l) + F(b_l) \tag{2}$$

where $F(x_i)$ is used as a skip connection to allow an unhindered flow of information through the network. $A(b_i)$ can be shown as:

$$A(b_l) : A_T\left(A_D([b_l, b_{l+1}, \ldots, b_{l+m}])\right) \tag{3}$$

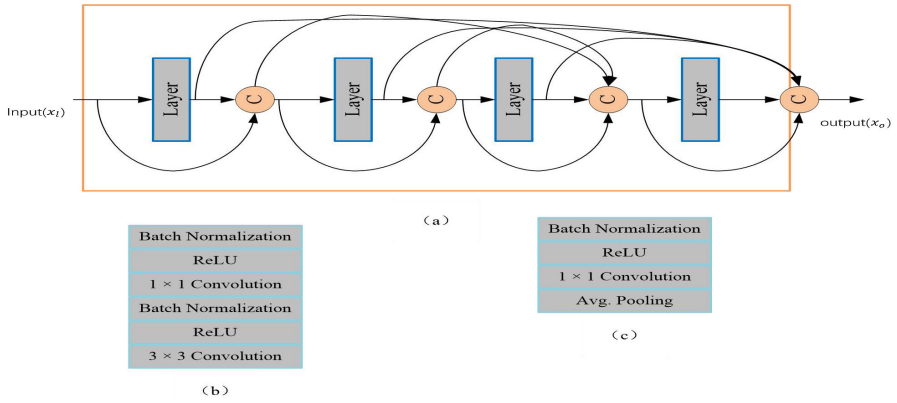

FIGURE 2. (a) New dense block (NDB); (b) operations in each layer of dense block; (c) operations in transition block; C concatenation.

A_T stands for the nonlinear function in the transition. b_{0-1} represents a nonlinear transformation of the outputs of the follow-up stacking layers in DBN.

$$b_{0-1} = A_D([b_l, b_{l+1}, \ldots, b_{l+m}]) \tag{4}$$

$A_D(.)$ is a layer shown in (b), which consists of batch normalization, ReLU, 1×1 convolution, batch normalization, ReLU, and 3×3 convolution. The DBN contains four layers in (a).

$A_T(.)$ is used in the transition operation with batch normalization, ReLU, 1×1 convolution, and pooling operation in (c). The space size of the output is reduced by a factor of 2 in each operation. Therefore. The addition of the elements of (3) applies a further downsampling operation during the skip. The feed to the second block includes a downsampled version of the raw data. It is already modified by a nonlinear function.

B. CONVOLUTION BLOCK ATTENTION MODULE

The CBAM [20] employs an attention mechanism to selectively improve multidimensional prostate features, extract features of interest in each layer and suppress more nonrelevant features. The network allows the creation of both channel and spatial awareness graphs through the exploitation of the channel-to-channel and space-to-space relationships of the characteristics respectively, which account for the " WHAT " and " WHERE " questions. The CBAM is composed of channel and spatial attention. The imported DWI is 2-channel K. CBAM specifies a one-dimensional channel attention graph B_C and spatial attention graph B_S [20], [21].

$$\begin{aligned} B_C(K) &= \sigma\left(MLP\left(AvgPool\ (K)\right) + MLP\left(MaxPool\ (K)\right)\right) \\ &= \sigma\left(W_1\left(W_0\left(K^c_{avg}\right)\right) + W_1\left(W_0(K^c_{\max})\right)\right) \end{aligned} \tag{5}$$

$$\begin{aligned} B_s(F) &= \sigma\left(g^{7\times7}([AvgPool(K); MaxPool(K)])\right) \\ &= \sigma(g^{7\times7}(K^s_{avg}; K^s_{\max})) \end{aligned} \tag{6}$$

where σ shows a common sigmoid function, $W_0 \in R^{(c/r\times c)}$, and $W_1 \in R^{(c/r\times c)}$. r indicates restoration ratio. The size of the activation layer belongs to $R^{C/r\times1\times1}$. Considering that MLP weights, W_0 and W_1 are shared for model inputs. ReLU is followed by W_0. pooling operation, k^c_{avg} and k^c_{max} are two spatial feature tools. $g^{(7\times7)}$ indicates a convolution operation and the size of the filter is 7×7.

The principle of attention is interpreted as follows:

$$K' = B_C(K) \otimes K \tag{7}$$

$$K'' = B_S(K') \otimes K' \tag{8}$$

$\otimes$ is the multiplication of representative elements. K″ refers to the model output.

C. CRF-RNN

Due to the limited capability of deep learning techniques in depicting objects, we introduce a type of convolution neural network. It is composed of a convolution neural network and probabilistic graphical model based on conditional random fields (CRF). CRF-RNN enacts a two-dimensional fully connected CRF as a recurrent neural network (RNN) [22]. The segmentation project is viewed as an optimizing task using CRF by minimizing function:

$$E(Y) = \sum\nolimits_{i=1}^{M} \emptyset(y_i^z) + \sum\nolimits_{\forall i,j,i<j} \omega(y_i^z, y_i^x) \tag{9}$$

where Y is the label of every pixel I_i. I is a 2D image. y_i^z shows target prediction of label z to image pixel I_i. y_j^x is the target prediction of label x to pixel, z, xϵL $= l_1 \ldots, l_c$ denotes task labels. Allocated costs of label u to I_i are measured by $\varphi(y_i^z)$. $\omega(y_i^z, y_i^x)$ is the allocation of the cost of labels z and x to I_i and I_j. Minimizing E(Y) to the function [20]:

$$\begin{aligned} F(Q) = \sum\nolimits_{\forall i,j,i<j} \sum\nolimits_{\forall z\in L} q_i^z q_i^x \omega(y_i^z, y_i^x) \\ + \sum\nolimits_{\forall i} \sum\nolimits_{\forall z\in L} q_i^z \ln q_i^z \end{aligned} \tag{10}$$

where q_i^z is the probability for label z to pixel.

$$q_i^z \propto \exp\{-\emptyset(y_i^z) - \sum\nolimits_{j,j\neq i} \sum\nolimits_{\forall x\in L} q_j^x \omega(y_i^z, y_i^x)\} \tag{11}$$

$$\omega(y_i^z, y_i^x) = \mu(z, x) \sum\nolimits_{m=1}^{K} w^m k^m(f_i, f_j) \tag{12}$$

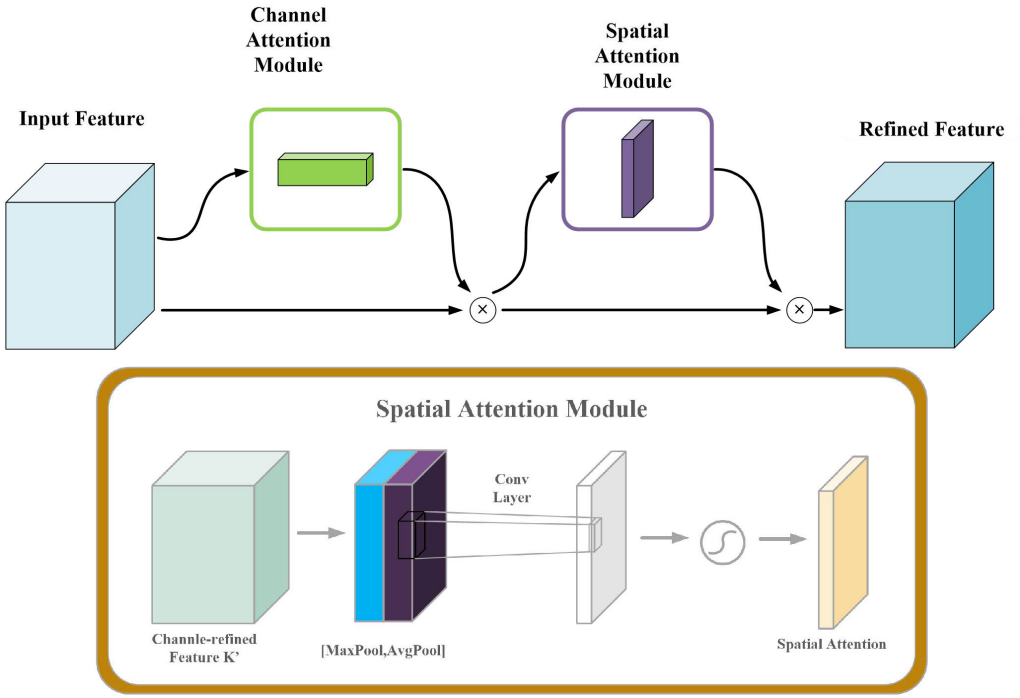

FIGURE 3. Convolution block attention module (CBAM). Channel attention module B_C, spatial attention module B_S.

The number of Gaussian kernels $k^{(m)}$ is 2. After the calculation of (4) and (3), the probability value is obtained:

$$q_i^z \propto \emptyset(y_i^z) - \exp\{\sum_{\forall x \in l} \mu(z,x) \sum_{m=1}^{K} W^m \sum_{m=1} k^m(f_i, f_j) q_j^x\} \tag{13}$$

Fully connected CRF forecasts the likelihood of a label to a pixel according to equation (13). q_i^z is computed with a mean-field iteration approach, formulated as RNN in order to allow CNNs and fully connected CRF to be incorporated into a single network. The crucial opinion of CRF as an RNN is that such an algorithm for inference may be composed of a series of steps [22]. CRF as an RNN layer can improve the quality of semantic segmentation with the gradient descent method [23].

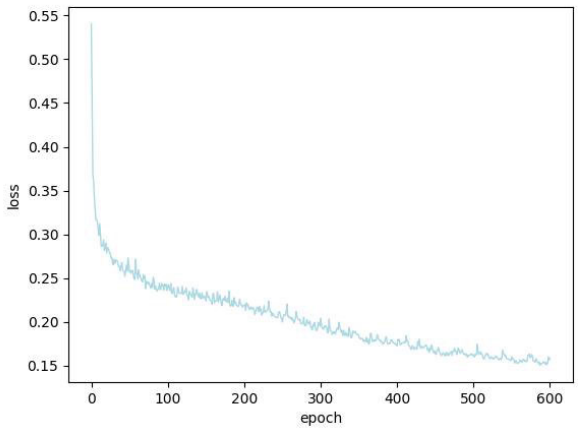

FIGURE 4. Changes in the loss on training data (our network).

IV. EVALUATION OF THE PROPOSED MODEL

We evaluated the network comparison with U-Net and its variant networks. FCN [24], U-Net [15], U-Net++ [25], ResU-Net [26]. Cross-entropy loss was used. The used optimization method was Adam since it converges faster. Each algorithm was retrained using real data sets. The number of iterations to reach convergence was different for each algorithm, and finally, we selected the best weights for each group to participate in the test comparison. Accuracy and Iou are also the most commonly used evaluation metrics to assess segmentation performance starting from a pixel classification perspective. Hausdorff distance mainly measures the degree of similarity points. Using 4 cross-validation approach, data was separated into a learning set (80%) and a testing set (20%). The size of the image was 256 × 256. Equipment configures included NVIDIA GTX 3090 × 8 and Ubuntu 64.

A. RESULTS

1) MODEL PERFORMANCE COMPARISON

a: LOSS VS EPOCH

As shown in Figures 4 and 5, the training session was recorded. These two charts show the different impact between the area of the prostate and the lesion on the epoch time. Epoch represents the completion of one round of training iterations. Figure 4 shows the loss trend of the prostate and its lesion segmentation. The loss value reduces substantially

TABLE 1. Comparison of segmentation performance of the prostate region for five models.

Model	Dice	Iou	Accuracy	Sensitivity	95%HD(mm)
U-Net	92.21%	85.82%	93.0%	92.33%	8.96
U-Net++	92.48%	84.90%	93.61%	91.02%	8.86
FCN	91.32%	84.61%	92.34%	91.91%	8.71
ResU-Net	86.70%	76.10%	89.50%	83.30%	8.51
Proposed	93.94%	85.85%	94.21 %	93.85%	7.80

TABLE 2. Comparison of segmentation performance of prostate lesion area for five models.

Model	Dice	Iou	Accuracy	Sensitivity	95%HD(mm)
U-Net	87.51%	77.91%	87.42%	88.50%	9.01
U-Net++	88.21%	77.45%	86.22%	87.53%	8.80
FCN	85.32%	75.04%	86.10%	85.01%	8.72
ResU-Net	81.20%	69.12%	86.30%	81.17%	8.68
Proposed	89.62%	78.30%	88.55%	89.39%	8.28

TABLE 3. Ablation experiments from our network for the segmentation of the prostate and its lesion regions (√ indications to implement this technology in the model).

	Backbone (U-Net with feature fusion)					
NDB	√	√	√		√	
CBAM	√	√		√		√
CRF-RNN	√		√	√		
Dice of Prostate/Prostate lesion regions	93.94%/89 .62%	93.70%/89 .34%	92.64%/87 .97%	89.91%/88 .98%	87.97%/ 87.77%	88.57%/ 86.64%

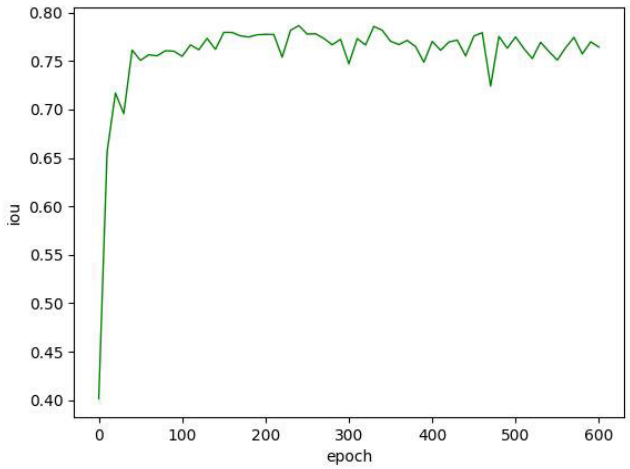

FIGURE 5. Changes in IOU on training data (our network).

at the beginning and the convergence slows down from 500 epochs. Later, as the amount of iterations grows, the model begins to converge.

b: IoU VS EPOCH

Given a set of images, the IoU measurement gives the similarity between the object prediction region and the ground truth region. Figure 5 gives the IoU variation of our model in the lesion region and the prostate region. In the beginning, our model IoU values are highly variable and oscillate up and down, especially between 400 epochs and 500 epochs. After that, the fluctuations slowly become smaller.

From each dimension, four cross-validations are used to calculate the segmentation performance of our model for the prostate and its lesion area. Table 1, the average dice score, Iou, accuracy, sensitivity, and 95%HD of the proposed network for the prostate are 93.94%, 85.85%, 94.21%, 93.85% and 7.80, respectively. Our network is superior to others. For example, U-Net, FCN, U-Net++ and ResU-Net were 1.21, 1.87,0.6, and 4.71 percent points lower than our network in accuracy for the prostate segmentation. In Table 2, the results of the presented network are better for the segmentation performance of prostate lesions in terms of Dice score 89.62%, Iou scores 78.30%, accuracy 88.55%, sensitivity 89.39%

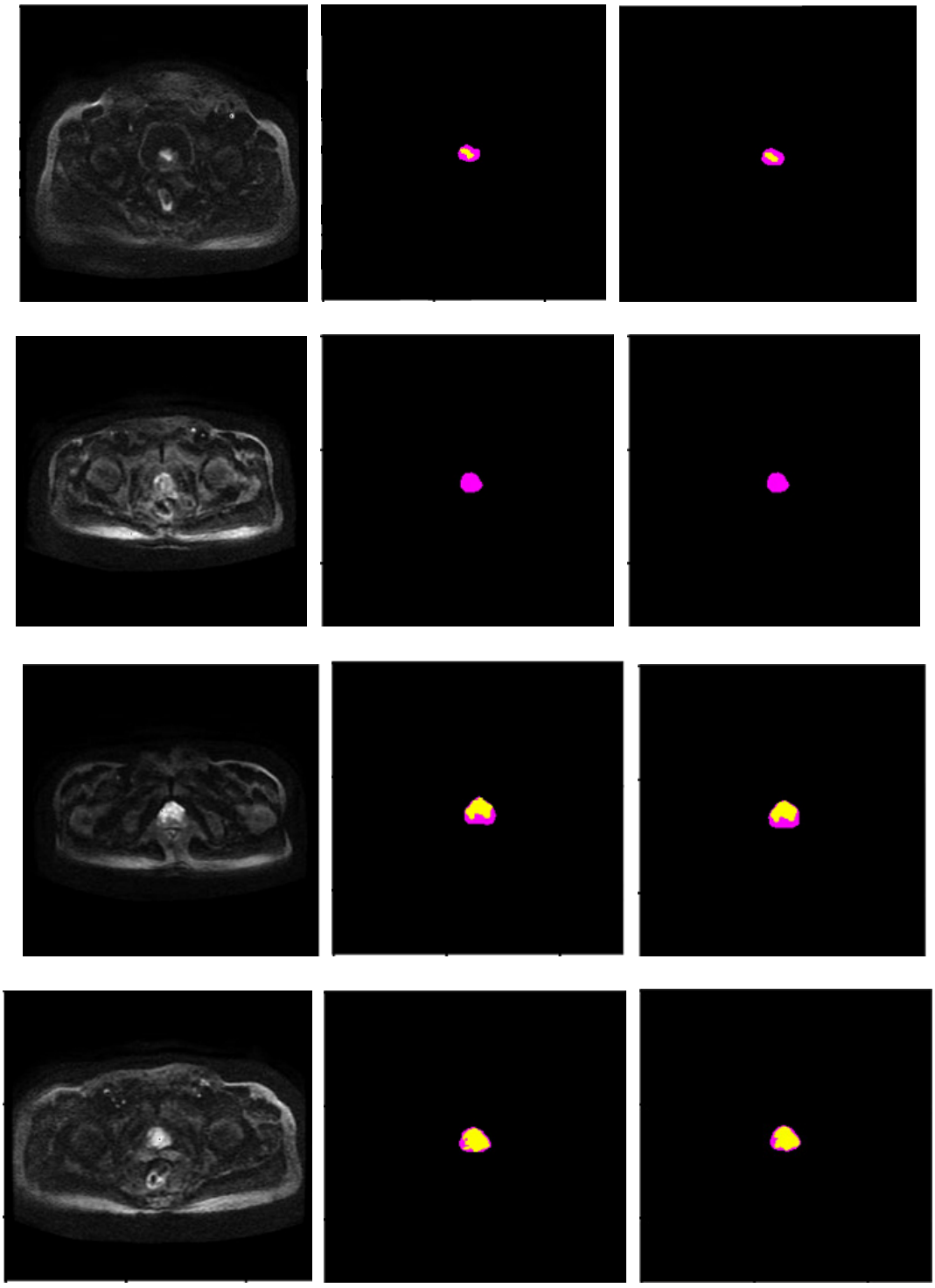

FIGURE 6. Segmentation performance of our network in four different samples. The column from left to right is the raw image, ground truth, and prediction images of our model. To make the results clearer, the non-targets (background) are masked in black.

and 95% HD 8.28 when compared to the rest of the four models.

The work contains ablation sets to test the influence of each module in Table 3. NDB, CBAM, and CRF-RNN are incrementally added to the underlying network. The experiment was executed with the same parameters, such as optimization strategies (Adam), batch size, learning rate, initialization, and loss function. From this table, we can see that each module has an important role in the segmentation. Our method obtains the optimal performance

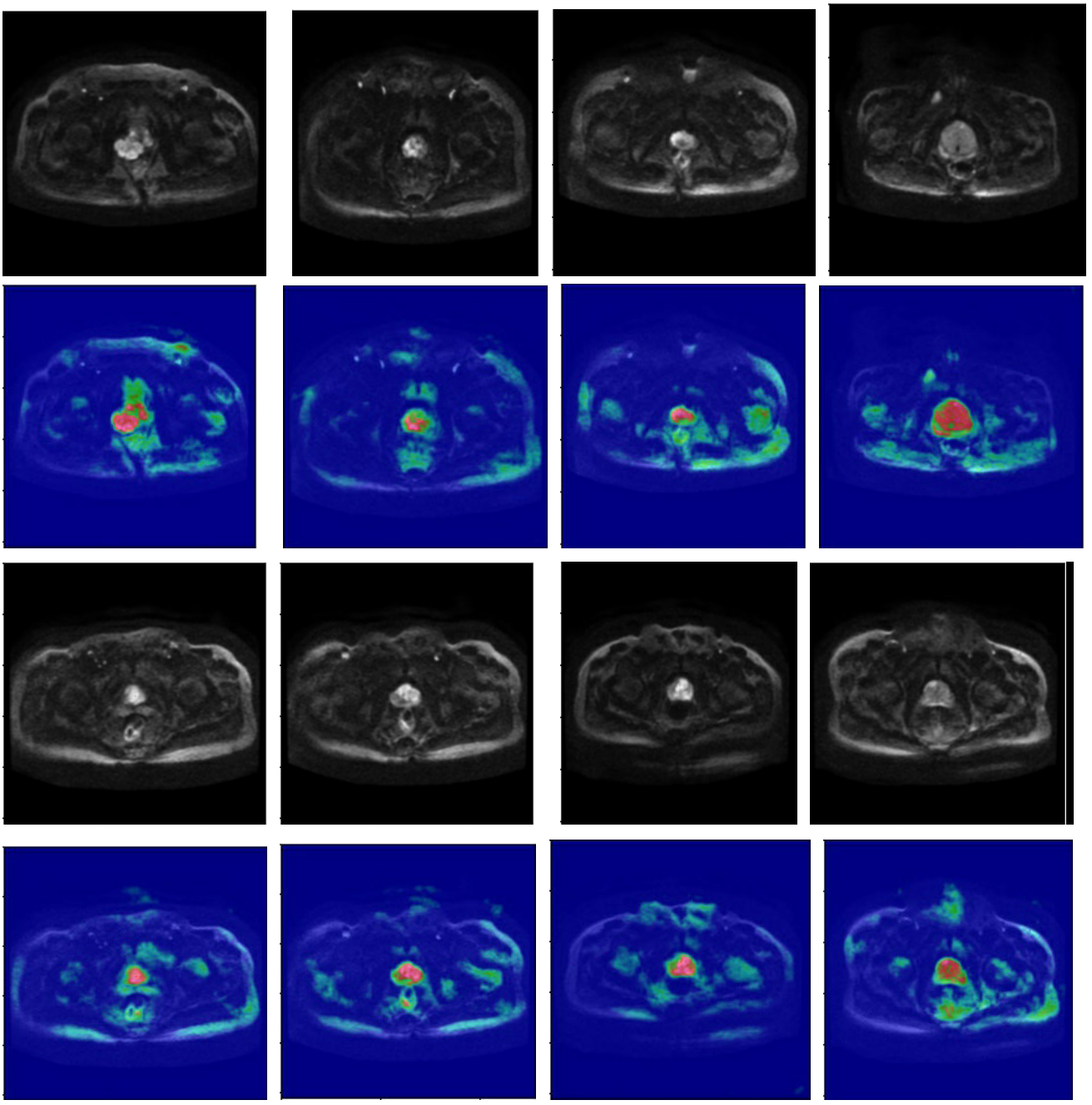

FIGURE 7. Visualization of the final layer of our model for prostate.

to learn more robust representations from NDB, CBMA and CRF-RNN.

2) VISUALIZATION OF SEGMENTATION RESULTS

The following images give a schematic of the segmentation results of our model in Figure.6. The picture below provides the segmentation outcome of our model in Figure 6. We have randomly chosen 4 samples from the test results to visualize the results. Consistent with the results shown in Tables 1 and Table 2, the performance of the prostate region is more sensitive than the discrimination of the lesion region. To illustrate the impact of the attention mechanism in our model, Figure 7 is presented to visualize the results of attention to the prostate lesion region in the last layer of the model. The red mask indicates the region of interest, i.e., the prostate lesion region.

V. DISCUSSION

To boost the performance of segmentation network and to aid in clinical management, a deep network with NDB

(New Dense Blocks) and CBAMs, CRF-RNN, was shown to take full advantage of the additional features encoded in different layers of the network to segment the prostate and the regions of disease. The performance of the model was evaluated on an actual data set. The experiments were designed to observe the loss and IOU variation during training, to compare the models' performance and to visualize the models' performance. Finally, we show that our proposed segmentation technique is superior to current techniques for prostate and lesion segmentation. The proposed technique showed excellent results, especially around the lesions, and this was highly relevant for clinical diagnosis and therapy.

Currently, many studies show that DCNN can be used to segment the prostate or to determine prostate cancer. Ding et al. [27] presented a method for recalibrating multilayer feature maps using multi-scale and channel self-attention (CSA). By embedding multi-scale features at the jump junction of the U-Net model (called UCAnet), they showed a consistent improvement in prostate segmentation in Dice, IoU, and ASSD. Duran et al. [28] demonstrated an innovative CNN model using an attention mechanism to segment PCa. This is like what we used to investigate. Furthermore, our model used CBAM for capturing spatial and channel features. A large number of effective features were extracted from this model for automatic and accurate segmentation of prostate lesions. We believe that the network has a few advantages.

First, our model is also devised with a synchronous structure, contracting and expanding paths, which are inspired by the classical model U-Net. In the network, copy and series connections are used in the same layer. The fusion of features is also present in different layers. This network is based on continuous in-depth feature extraction of prostate features using a systolic network. Meanwhile, the extended network is used to fill in the lacking images of the reduced network. To better exploit the underlying image information, we merge the lower sampled features with the upper layer features.

Second, the new dense blocks are added to the down-sampleing phase of the model to efficiently preserve and propagate the prostate and the characteristics of the lesions. In the symmetric up-adaptation phase, an attention mechanism is introduced that allows the model to focus on the features of the prostate in two dimensions: the spatial dimension and the channel dimension. In general, the prediction results are affected by the large number of parameters in the DCNN model. DNB and CBAM being consolidated into the model do not increase the parameter burden of the network but can improve the segmentation performance [20], [23]. CRF-RNN is placed at the end of the model to improve the semantic quality of the segmentation.

Third, several depth networks for prostate cancer identification use a composite of image series as input [15], [29], [30] or the model adopts a multi-transverse output [31], [32]. The deeper the model, the more training instances are needed and the higher the risk of overfitting. In comparison, our model also produces good results using a simple image input and a branch output.

There are some limitations of our study: (1) In deep learning, it is more data means more output. The data used to train the models was limited. (2), The running speed of the network could also be raised. For example, considering optimizing the algorithm or the tuning strategy, etc. (3), Initializing the parameters will have an enormous effect on the results of the model. For the parameter model, we use a random initialization. For the convergence of the model, an effective initialization is more beneficial. Clinical applications require more demanding models, such as the requirement of robustness and real-time. In the future, we will continue to expand the prostate data, and on the other hand, the joint use of MRI data in a variety of formats can bridge the shortcomings of a single input and increase the segmentation outcome of the prostate and lesion regions.

VI. CONCLUSION

In conclusion, for the segmentation of the prostate and its diseased area, we propose a new segmentation model which incorporates a new dense block, a convolution block attention module and CRF-RNN techniques. Experimental results show that this automatic segmentation model has a better performance compared to other models, supporting its promising potential to supplement the detection and treatment of prostate diseases in clinical medicine.

REFERENCES

[1] N. Aldoj, S. Lukas, M. Dewey, and T. Penzkofer, "Semi-automatic classification of prostate cancer on multi-parametric MR imaging using a multi-channel 3D convolutional neural network," *Eur. Radiol.*, vol. 30, no. 2, pp. 1243–1253, Feb. 2020.

[2] J. Ferlay, M. Colombet, I. Soerjomataram, D. M. Parkin, M. Piñeros, A. Znaor, and F. Bray, "Cancer statistics for the year 2020: An overview," *Int. J. Cancer*, vol. 149, no. 4, pp. 778–789, Aug. 2021.

[3] Y. Wang, Z. Deng, X. Hu, L. Zhu, X. Yang, X. Xu, and D. Ni, "Deep attentional features for prostate segmentation in ultrasound," in *Proc. 21st Int. Conf. MICCAI*, Granada, Spain, Sep. 2018, pp. 523–530.

[4] T. Brosch, J. Peters, A. Growth, T. Stehle, and J. Weese, "Deep learning-based boundary detection for model-based segmentation with application to MR prostate segmentation," in *Proc. 21st Int. Conf. MICCAI*, Granada, Spain, Sep. 2018, pp. 515–522.

[5] M. Woźniak, M. Wieczorek, and J. Siłka, "BiLSTM deep neural network model for imbalanced medical data of IoT systems," *Future Gener. Comput. Syst.*, vol. 141, pp. 489–499, Apr. 2023.

[6] J. Chaki and M. Woźniak, "Deep learning for neurodegenerative disorder (2016 to 2022): A systematic review," *Biomed. Signal Process. Control*, vol. 80, Feb. 2023, Art. no. 104223.

[7] M. Wu and L. Chen, "Image recognition based on deep learning," in *Proc. Chin. Autom. Congr. (CAC)*, Nov. 2015, pp. 542–546.

[8] O. Ronneberger, P. Fischer, and T. Brox, "U-Net: Convolutional networks for biomedical image segmentation," in *Proc. Med. Image Comput. Comput.-Assist. Intervent.*, 2015, pp. 234–241.

[9] F. Isensee, P. F. Jaeger, S. A. A. Kohl, J. Petersen, and K. H. Maier-Hein, "NnU-Net: A self-configuring method for deep learning-based biomedical image segmentation," *Nature Methods*, vol. 18, no. 2, pp. 203–211, Feb. 2021.

[10] M. Rajchl, M. C. H. Lee, O. Oktay, K. Kamnitsas, J. Passerat-Palmbach, W. Bai, M. Damodaram, M. A. Rutherford, J. V. Hajnal, B. Kainz, and D. Rueckert, "DeepCut: Object segmentation from bounding box annotations using convolutional neural networks," *IEEE Trans. Med. Imag.*, vol. 36, no. 2, pp. 674–683, Feb. 2017.

[11] A. Top, G. Hamarneh, and R. Abugharbieh, "Active learning for interactive 3D image segmentation," in *Proc. 14th Int. Conf. MICCAI*. Berlin, Germany: Springer, 2011, pp. 603–610.
[12] G. Wang, M. A. Zuluaga, W. Li, R. Pratt, P. A. Patel, M. Aertsen, T. Doel, A. L. David, J. Deprest, S. Ourselin, and T. Vercauteren, "DeepIGeoS: A deep interactive geodesic framework for medical image segmentation," *IEEE Trans. Pattern Anal. Mach. Intell.*, vol. 41, no. 7, pp. 1559–1572, Jul. 2019.
[13] L. Geng, S. Li, Z. Xiao, and F. Zhang, "Multi-channel feature pyramid networks for prostate segmentation, based on transrectal ultrasound imaging," *Appl. Sci.*, vol. 10, no. 11, p. 3834, May 2020.
[14] M. Arif, I. G. Schoots, J. C. Tovar, C. H. Bangma, G. P. Krestin, M. J. Roobol, W. Niessen, and J. F. Veenland, "Clinically significant prostate cancer detection and segmentation in low-risk patients using a convolutional neural network on multi-parametric MRI," *Eur. Radiol.*, vol. 30, no. 12, pp. 6582–6592, Dec. 2020.
[15] H. Zunair and A. B. Hamza, "Sharp U-Net: Depthwise convolutional network for biomedical image segmentation," *Comput. Biol. Med.*, vol. 136, Sep. 2021, Art. no. 104699.
[16] X. Xu, F. Zhou, and B. Liu, "Automatic bladder segmentation from CT images using deep CNN and 3D fully connected CRF-RNN," *Int. J. Comput. Assist. Radiol. Surg.*, vol. 13, no. 7, pp. 967–975, Jul. 2018.
[17] A. D. Gleed, Q. Chen, J. Jackman, D. Mishra, V. Chandramohan, A. Self, S. Bhatnagar, A. T. Papageorghiou, and J. A. Noble, "Automatic image guidance for assessment of placenta location in ultrasound video sweeps," *Ultrasound Med. Biol.*, vol. 49, no. 1, pp. 106–121, Jan. 2023.
[18] K. Xu, Y. Zhao, F. Li, and W. Xiang, "Single infrared image stripe removal via deep multi-scale dense connection convolutional neural network," *Infr. Phys. Technol.*, vol. 121, Mar. 2022, Art. no. 104008.
[19] D. Song, C. Xu, X. Jia, Y. Chen, C. Xu, and Y. Wang, "Efficient residual dense block search for image super-resolution," in *Proc. AAAI Conf. Artif. Intell.*, 2020, vol. 34, no. 7, pp. 12007–12014.
[20] S. Woo, J. Park, J. Y. Lee, and I. S. Kweon, "CBAM: Convolutional block attention module," in *Proc. Eur. Conf. Comput. Vis. (ECCV)*, 2018, pp. 3–19.
[21] C. Chen, B. Wu, and H. Zhang, "An image recognition technology based on deformable and CBAM convolution ResNet50," *Int. J. Comput. Sci.*, vol. 50, no. 1, pp. 1–8, 2023.
[22] S. Zheng, S. Jayasumana, B. Romera-Paredes, V. Vineet, Z. Su, D. Du, C. Huang, and P. H. S. Torr, "Conditional random fields as recurrent neural networks," in *Proc. IEEE Int. Conf. Comput. Vis. (ICCV)*, Dec. 2015, pp. 1529–1537.
[23] M. Monteiro, M. A. T. Figueiredo, and A. L. Oliveira, "Conditional random fields as recurrent neural networks for 3D medical imaging segmentation," 2018, *arXiv:1807.07464*.
[24] J. Long, E. Shelhamer, and T. Darrell, "Fully convolutional networks for semantic segmentation," in *Proc. IEEE Conf. Comput. Vis. Pattern Recognit. (CVPR)*, Jun. 2015, pp. 3431–3440.
[25] Z. Zhou, M. M. R. Siddiquee, N. Tajbakhsh, and J. Liang, "UNet++: A nested U-Net architecture for medical image segmentation," in *Deep Learning in Medical Image Analysis and Multimodal Learning for Clinical Decision Support: 4th International Workshop, DLMIA 2018, and 8th International Workshop, ML-CDS 2018, Held in Conjunction With MICCAI 2018, Granada, Spain, September 20, 2018, Proceedings*. Springer, 2018, pp. 3–11.
[26] D. Jha, P. H. Smedsrud, D. Johansen, T. de Lange, H. D. Johansen, P. Halvorsen, and M. A. Riegler, "A comprehensive study on colorectal polyp segmentation with ResUNet++, conditional random field and test-time augmentation," *IEEE J. Biomed. Health Informat.*, vol. 25, no. 6, pp. 2029–2040, Jun. 2021.
[27] M. Ding, Z. Lin, C. H. Lee, C. H. Tan, and W. Huang, "A multi-scale channel attention network for prostate segmentation," *IEEE Trans. Circuits Syst. II, Exp. Briefs*, vol. 70, no. 5, pp. 1754–1758, May 2023.
[28] A. Duran, G. Dussert, O. Rouvière, T. Jaouen, P.-M. Jodoin, and C. Lartizien, "ProstAttention-Net: A deep attention model for prostate cancer segmentation by aggressiveness in MRI scans," *Med. Image Anal.*, vol. 77, Apr. 2022, Art. no. 102347.
[29] Y. Song, Y. Zhang, X. Yan, H. Liu, M. Zhou, B. Hu, and G. Yang, "Computer-aided diagnosis of prostate cancer using a deep convolutional neural network from multiparametric MRI," *J. Magn. Reson. Imag.*, vol. 48, no. 6, pp. 1570–1577, Dec. 2018.
[30] R. Cao, X. Zhong, S. Afshari, E. Felker, V. Suvannarerg, T. Tubtawee, S. Vangala, F. Scalzo, S. Raman, and K. Sung, "Performance of deep learning and genitourinary radiologists in detection of prostate cancer using 3-T multiparametric magnetic resonance imaging," *J. Magn. Reson. Imag.*, vol. 54, no. 2, pp. 474–483, Aug. 2021.
[31] Y. Chen, L. Xing, L. Yu, H. P. Bagshaw, M. K. Buyyounouski, and B. Han, "Automatic intraprostatic lesion segmentation in multiparametric magnetic resonance images with proposed multiple branch UNet," *Med. Phys.*, vol. 47, no. 12, pp. 6421–6429, Dec. 2020.
[32] Y. Zhu, R. Wei, G. Gao, L. Ding, X. Zhang, X. Wang, and J. Zhang, "Fully automatic segmentation on prostate MR images based on cascaded fully convolution network," *J. Magn. Reson. Imag.*, vol. 49, no. 4, pp. 1149–1156, Apr. 2019.

CHENGJUAN REN received the master's degree in computer software and theory from Chongqing University, Chongqing, China, in 2010, and the Ph.D. degree in software convergence engineering from Kunsan National University, Gunsan, South Korea, in 2022. She is currently a Professor with the College of Language Intelligence, Sichuan International Studies University, Chongqing. She is the Dean of the School of Computer Science. Her main research interests include machine learning, deep learning, and artificial intelligence. She is a member of the Intelligent Ecology Technical Group of the Internet of Things Committee of the Chinese Society of Communication and the Executive Director of the Shaanxi Computer Education Society.

HUIPENG REN received the bachelor's degree in medical imaging from North Sichuan Medical College, Nanchong, Sichuan, China, in 2008, and the master's degree in imaging medicine and nuclear medicine from Xi'an Jiaotong University, Xi'an, Shaanxi, China, in 2017. He is currently engaged in medical imaging diagnosis with the Department of Medical Imaging, Baoji Central Hospital, Shaanxi. He is an Associate Chief Physician. His research interests include the clinical application of new magnetic resonance technology, imaging diagnosis of abdominal and pelvic tumors, deep learning, and prostate MRI segmentation.